Robust graphene-based molecular devices

Maria El Abbassi,[1,2,3] Sara Sangtarash,[4] Xunshan Liu,[5] Mickael Lucien Perrin,[1] Oliver Braun,[1,6] Colin Lambert,[4] Herre Sjoerd Jan van der Zant,[3] Shlomo Yitzchaik,[7] Silvio Decurtins,[5] Shi-Xia Liu,[5,*] Hatef Sadeghi,[4,8,†] and Michel Calame[1,2,9,‡]

[1]*Empa, Swiss Federal Laboratories for Materials Science and Technology, Transport at nanoscale interfaces Laboratory, CH-8600 Dübendorf, Switzerland.*

[2]*Department of Physics, University of Basel, Klingelbergstrasse 82, CH-4056 Ba-sel, Switzerland*

[3]*Kavli Institute of Nanoscience, Delft University of Technology, Lorentzweg 1, 2628 CJ Delft, The Netherlands*

[4]*Department of Physics, Lancaster University, Lancaster LA1 4YB, United Kingdom*

[5]*Department of Chemistry and Biochemistry, University of Bern, 3012 Bern, Switzerland*

[6]*Department of Physics, University of Basel, Klingelbergstrasse 82, CH-4056 Basel, Switzerland*

[7]*Institute of Chemistry, The Hebrew University of Jerusalem, Jerusalem, 91904, Israel*

[8]*School of Engineering, University of Warwick, Coventry, CV4 7AL, United Kingdom*

[9]*Swiss Nanoscience Institute, University of Basel, 4056 Basel, Switzerland.*

One of the main challenges to upscale the fabrication of molecular devices is to achieve a mechanically stable device with reproducible and controllable electronic features, operating at room temperature[1,2]. This is crucial because structural and electronic fluctuations can lead to significant changes in the transport characteristics at the electrode-molecule interface[3,4]. In this study, we report on the realization of a mechanically and electronically robust graphene-based molecular junction. Robustness is achieved by separating the requirements for mechanical and electronic stability at the molecular level. Mechanical stability is obtained by anchoring molecules directly to the substrate, rather than to graphene electrodes, using a silanization reaction. Electronic stability is achieved by adjusting the π-π orbitals overlap of the conjugated head groups between neighbouring molecules. The molecular devices exhibit stable current-voltage (I-V) characteristics up to bias voltages of 2.0 V with reproducible transport features in the temperature range from 20 K to 300 K.

To realize reliable graphene-based junctions, several issues exist to date and need to be addressed. First, graphene-based junctions have been reported to exhibit signatures similar to those of molecules, with gate-dependent resonance features, such as Coulomb blockade[5,6], quantum interference[7] and Fabry-Perrot resonances[8]. Second, connecting molecules to the graphene remains challenging due to the lack of control on the electrode geometry at the nanoscale[4,5,8–10]. Achieving both mechanical stability and electrical reproducibility at the same time impose different requirements on the junction properties[3,11]. Finding the proper balance between electronic and mechanical stability is therefore challenging. Weakly coupled $\pi - \pi$ stacking is believed to be an appealing strategy to anchor molecules to the contact electrodes[3], offering advantages such as high thermoelectric efficiency. However, this approach has been shown to lead to mechanically unstable junctions[12]. Alternatively, molecules have also been bonded covalently to graphene, yielding mechanically stable junctions[10]. However, transport through strongly coupled molecules is expected to be heavily influenced by the electrode geometry, edge termination and crystallographic structure, leading to a large variability in the shape of the current-voltage characteristics[3]. Third, junction-to-

junction variability remains high for the above-mentioned anchoring methods[13,14], leading to poor devices reproducibility. Finally, the silicon dioxide substrate itself has been reported to yield feature-rich charge-transport characteristics[15], in particular due to switching within the oxide[16], which may be confused with molecular signatures.

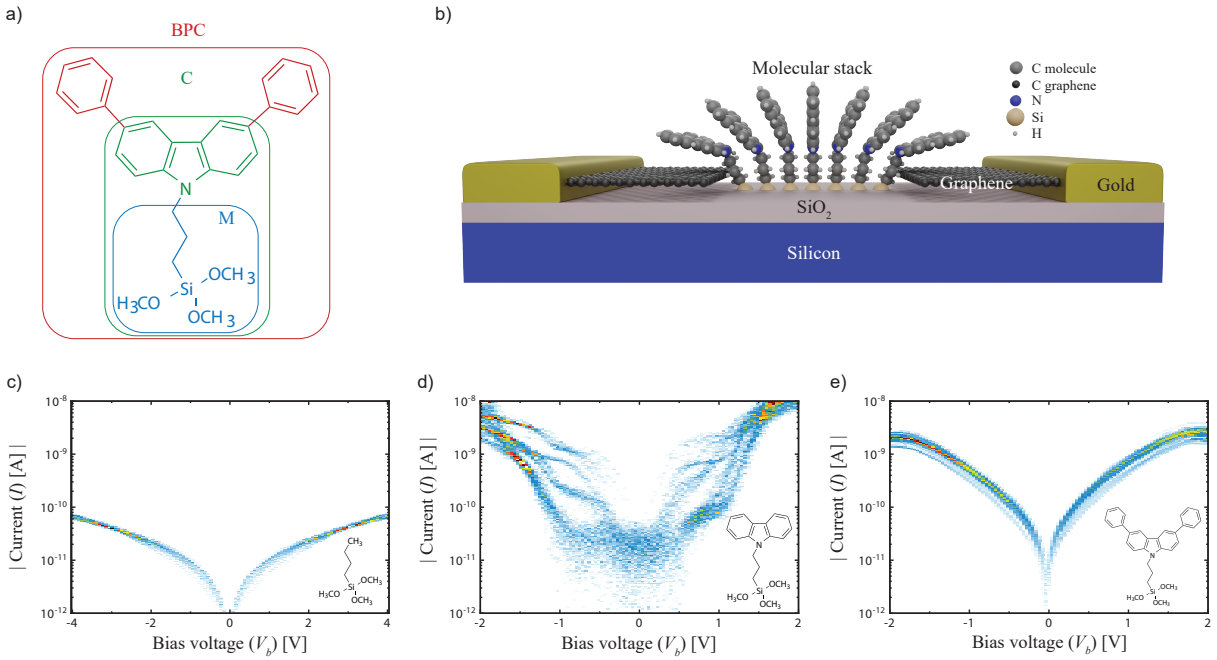

Figure 1: **Junction geometry, molecular design and electrical characterization.** a) Drawing of the three molecules, constituted of three main parts: the silane group for the covalent anchoring to the substrate, the alkane chain that decouples the silane group from the different head groups : CH_3 (molecule M) , N-carbazole (molecule C), and bi-phenyl N-carbazole (molecule BPC). b) Schematic illustration of a molecular junction containing a series of π-π-stacked molecules bridging a graphene nanogap. The atomic positions of the molecules are for illustrative purposes only, and do not correspond to the DFT-relaxed geometry shown in Figure 4. For clarity reasons, different atoms and colours are used to distinguish carbon atoms of the molecule from those of the graphene. c-e) The electrical measurements corresponding to the three molecules under study with different head groups are displayed as density plots of the measured I-V curves, of which the absolute value of the current is plotted on logarithmic scale. For each molecule, 100 I-V curves without data selection are measured at room temperature on a specific device per molecule.

The molecule we propose (see Fig. 1a) contains three main parts, a silane group and a π-conjugated head group, decoupled by a non-conjugated alkane chain. The silane part is responsible for the mechanical anchoring of the molecule by forming a covalent bond with the substrate. This silanization process is commonly used to cover surfaces with organofunctional molecules[17–19]. This approach offers distinct advantages. As the graphene edges usually present ill-defined edge terminations after nanofabrication and/or preparation of the

contact electrodes, anchoring the molecules to the substrate seems a valid possible alternative. In addition, as the molecules are covalently bonded to the substrate, this process leads to mechanically stable graphene-molecule junctions. Moreover, the silanization process also passivates the silicon dioxide surface and prevents unwanted switching effects[16]. The second part of the molecule is the conjugated head group, specifically a bi-phenyl N-carbazole group (molecule BPC), whose orbitals can couple to the π orbitals of the graphene. The alkane chain is the final necessary element, whose crucial role is to electronically decouple the mechanical anchoring from the electronic head group. Density functional theory (DFT) calculations (methods and Supplementary Information SI section II) confirm that the frontier orbitals of the BPC molecule are indeed solely localized on the head group. These calculations also show that head groups of two neighbouring molecules can $\pi - \pi$ stack, forming transport channels which are delocalized across all head groups. A schematic illustration of BPC molecules assembled in the graphene nanogap with $\pi - \pi$ stacked head groups is shown in Fig. 1b).

In order to correlate the junction stability and electrical properties with the molecular structure, several test molecules with different head groups were designed and investigated. The first test molecule is methyl terminated (abbreviated as molecule M). Due to the absence of a delocalized π system, it is expected to only poorly conduct charges. The second test molecule possess an N-carbazole head group (abbreviated as molecule C). The π-system of molecule C has two phenyl rings less than the BPC molecule. The lack of phenyl rings leads to a reduction in orbital overlap by about a factor of two, resulting in a lower interaction energy between neighbouring head groups[3]. Due to its smaller interaction energy, molecule C is therefore expected to form less stable transport channels than the BPC molecule.[3]A description of the device fabrication and molecule deposition can be found in the Methods section.

Figure 1c)-e) presents the electrical characterisation of three devices, each exposed to one of the molecules under study. For this purpose, current-voltage characteristics (I-V curves) are acquired at room temperature by averaging a back-and-forth voltage sweep. For each device, 100 I-V curves are measured and combined into a density plot without any data selection. This density plot consists of a 2-dimensional histogram of all I-V curves recorded on the device, constructed by binning both the current and the voltage axes. For the current axis, the absolute value of the current on log-scale is used. The density plots are a color-

coded representation of such histograms, in which areas of high counts can be identified, corresponding to the most likely device behaviour. The density plots are normalized by the total number of data points.

The junction containing molecule M (Fig. 1c) presents a single category of tunnelling-like I-V curves, with a maximum current of about 10 pA at a bias voltage of 2 V. The I-V curves recorded on junctions exposed to molecule C are shown in Fig. 1d. The maximum currents are about two orders of magnitude larger than for molecule M, indicating that the π-π stacking leads to a more efficient charge transport across the molecular junction. However, the plot also exhibits large variations in I-V shapes and current levels. These fluctuations are attributed to the weak electronic interaction between the neighbouring head groups, allowing for various molecular conformations to occur, each of them possibly with slightly different electronic properties (a more detailed study is presented in the SI section III). Figure 1e shows the density plot of the I-V curves recorded for a device after deposition of molecule BPC. Contrary to molecule C, the BPC molecule leads to both a higher current and a higher stability, as shown by the high similarity of the 100 I-V curves recorded at room temperature.

Stability and intersample reproducibility at 20 K

We performed electrical measurements at cryogenic temperatures (20 K) to spectroscopically characterize the BPC molecular junctions. Figure 2 presents an overview of these measurements, with Fig. 2a showing three individual I-V curves recorded on each device. 100 of such I-V curves are measured successively. The 100 I-V curves are then used to construct a density plot (Fig. 2b), as described previously. Here, only one category of I-V curves is observed, with small fluctuations. Furthermore, all devices exhibit similar current levels (within one order of magnitude) and curve shape. The inset shows the corresponding average I-V curve ($\langle I \rangle$), exhibiting a very similar shape as the individual I-V curves shown in Fig. 2a. Finally, the numerical derivative of $\langle I \rangle$ is calculated (Fig. 2c) in order to obtain the differential conductance ($\mathrm{d}\langle I \rangle/\mathrm{dV}$) traces (blue line). As a comparison, the red traces display the dI/dV curve for that particular device obtained at 20 K before deposition. The observed resonance peaks are a signature of one or more transport channels present in the molecular junction. As these resonances are only present after deposition of molecules,

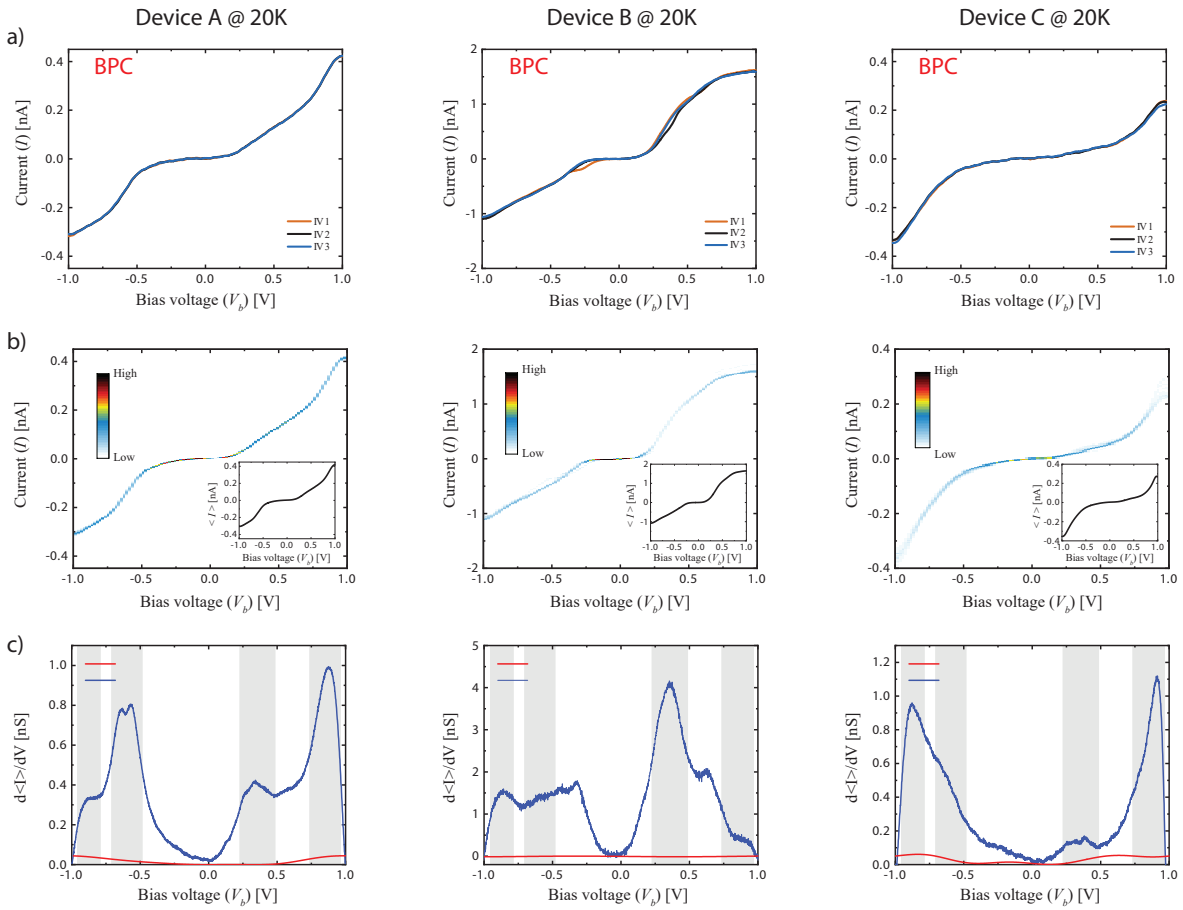

Figure 2: **Electrical characterization of devices A-C at 20 K exposed to molecule BPC.** a) Three individual I-V curves recorded for each device. b) Density plots of I-V curves. The inset shows the average I-V curve $\langle I \rangle$. c) $\mathrm{d}\langle I \rangle/\mathrm{dV}$ curve obtained before (red) and after (blue) deposition. The resonances observed after deposition correspond to electronic energy levels of the molecular junction. The grey regions highlight the different resonances.

they are attributed to the presence of the BPC molecule. In general, the position of these resonances reflects the electronic structure of the junction. These resonances are located at similar bias voltages, highlighted by the grey-shaded regions, confirming the robustness and reproducibility of the BPC molecular junctions. We note, however, that the resonances exhibit different amplitudes, which may be attributed to local variations in the junction conformation.

Finally, we note that also for molecule C, the mechanical anchoring to the substrate is stable, even though the electronic transport is not. In the Supporting Information, using a statistical cross-correlation analysis, we show that similar electronic features are observed across multiple devices, demonstrating that indeed the anchoring to the substrate provides

sufficient mechanical stability. However, due to the smaller π-π overlap between the head groups compared to the BPC molecule, the electronic stability is limited.

Electronic robustness of the junctions at different temperatures

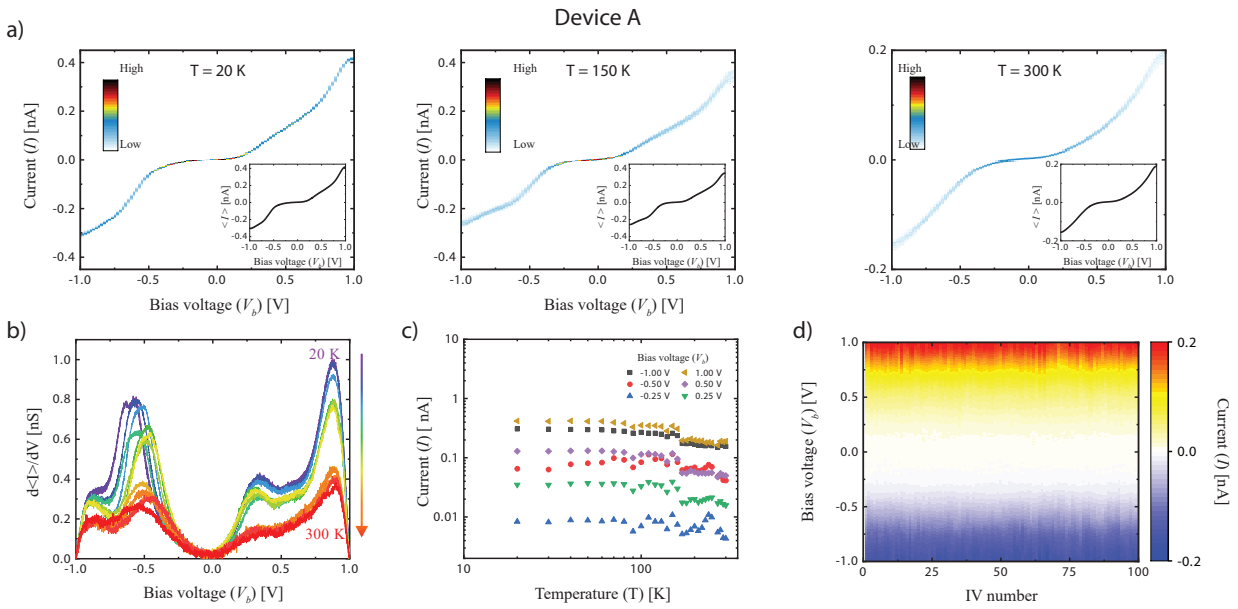

Figure 3: **Transport measurements through a BPC molecular junction (device A) at different temperatures.** a) Density plots constructed from 100 I-V curves for the three temperatures. b) Differential conductance $d\langle I\rangle/dV$ of the device shown in a) plotted for increasing temperatures. c) Evolution of the absolute value of $\langle I\rangle$ as a function of the temperature plotted for different bias values in log-log scale. d) Evolution over time of the I-V curves measured at 300 K.

We further investigate the junction stability by characterizing the devices in a large range of temperature extending from 20 K to room temperature. Figure 3a shows the density plot obtained from 100 I-V curves measured at three selected temperatures (20 K, 150 K and 300 K) for device A, with $\langle I\rangle$ as inset. From the density plots, the high similarity between successive I-V curves is observed at all temperatures. This behaviour highlights the high electronic and mechanical stability of the devices, in stark contrast to the behaviour of junctions based on molecule C (Fig. 1d). A similar observation can also made in Fig. 3b. Here, the plot shows the evolution of d$\langle I\rangle$/dV with temperature. The resonance positions remain fairly similar throughout the entire range, while the peak amplitude steadily decays with increasing temperature.

Figure 3c presents the evolution of $\langle I\rangle$ as a function of temperature, plotted in a

logarithmic scale. The plot shows that the current remains fairly constant over the entire temperature range for various bias voltage values, and in particular in the high temperature region between 150 K and 300 K. This observation suggests that charge transport though these graphene-molecule-graphene junctions remains coherent up to 300 K. This appealing effect is in contrast with studies performed in systems in which electrons are transported incoherently through the device. In that case a strong reduction in current is observed for decreasing temperatures, corresponding to activation energies in the 10-100 meV range[20–25]. Interestingly, the current through our device even increases slightly with decreasing temperature. This effect may be related to minor rearrangements of the molecules in the junction, which may also be the cause for the small jump in current measured around 120 K. The temperature dependence of the empty graphene gaps was also investigated (see Supporting Information for more details), but no significant effect of temperature was observed, in agreement with a previous study[9]. Finally, Fig. 3d presents the evolution of the I-V curves over time at room temperature. Here, no significant fluctuations were observed at bias values up to 2.0 V, highlighting the very high stability of the molecular junctions.

To investigate charge transport through these graphene/molecule/graphene junctions, we calculated the transmission probability $T(E)$ of electrons with energy E passing through the molecules from one graphene electrode to another (see methods). We obtain the material specific mean-field Hamiltonian from the SIESTA implementation of density functional theory[26] combined with the Gollum implementation of the non-equilibrium Green's function method to calculate $T(E)$[27] (see computational method). The conductance G was calculated for different Fermi energies and temperatures using the Landauer formula: $G = G_0 \int dE T(E)(-df/dE)$ where $f = (1 + exp((E - E_F)/K_B\mathrm{T}))^{-1}$ is the Fermi Dirac distribution function, T is the temperature, and $k_B = 8.6 \times 10^{-5} eV/K$ is Boltzmann's constant.

Figure 4 shows the computed conductance (G/G_0) for reference molecule M and molecule BPC for a particular junction geometry. Transmissions were also calculated for other geometries (see SI section II). The calculations show that the transmission through the reference molecules is systematically lower than for the BPC molecule, regardless of the choice of the Fermi energy. This observation also holds for other junction configurations (see SI section II). The drastically lower conductance is attributed to the HOMO-LUMO gap of the

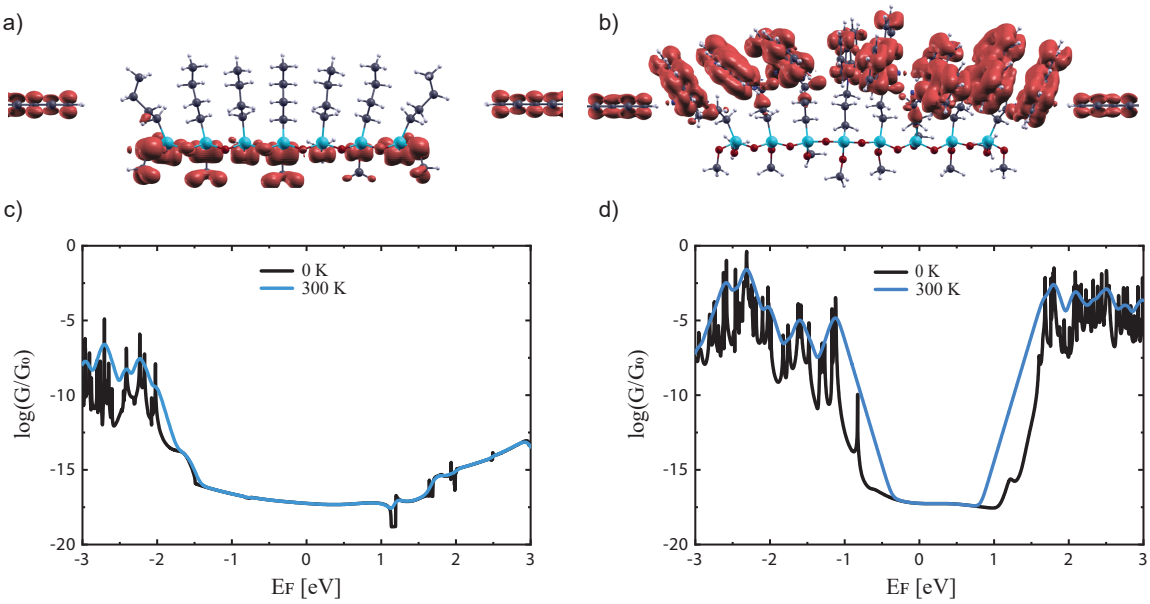

Figure 4: **Transport through graphene/molecule/graphene junctions containing the M and BPC molecule.** (a,b) Computed conductance (G/G_0) of a junction containing molecules M for different Fermi energies (E_F) at T = 0 K and T = 300 K. Local density of states (LDOS) for the shaded region in (b) showing that the wave function does not extended over the alkane groups. (c,d) Computed conductance (G/G_0) of a junction containing molecules BPC for different Fermi energies (E_F) at T = 0 K and T = 300 K. Local density of states (LDOS) for the shaded region in (d) shows that wave function is extended over the carbazole groups. Note that E_F is the Fermi energy of the junctions relative to the DFT predicted Fermi energy, and may be different from the experiments. The grey-shaded area corresponds to the resonance closest to the Fermi energy of the electrodes.

graphene/molecule/graphene junction being larger for reference molecule M. To investigate the nature of the transport channels dominating transport for both molecule, Fig. 4a and 4c display the local density-of-states obtained in the energy window highlighted in grey, corresponding to the resonance closest to the Fermi energy. For the BPC molecule, the wave function extends over the bi-phenyl N-carbazole groups. For the reference molecule, on the other hand, no delocalized orbitals are formed and transport occurs via the poorly conducting silane groups. These calculations demonstrate the crucial role of $\pi - \pi$ stacked head groups in the transport, and rationalize the large difference in current observed experimentally for the two molecules.

We have reported on graphene-based molecular devices which are electronically and mechanically stable over a large temperature range. This is achieved by decoupling the mechanical anchoring from the electronic pathways by combining a covalent binding of the

molecules to the substrate and large π-conjugated head groups. The junctions are reproducible throughout several devices and operate from 20 K up to room temperature. Our approach represents a simple but powerful strategy for the future integration of molecule-based functions into stable and controllable nano-electronic devices.

Methods

Molecular synthesis: M and C molecules were purchased from Sigma-Aldrich. Details of the synthesis of the BPC molecule are presented in the supplementary information section I.

Junction formation: The molecular junctions were formed as follows. First, nanogaps were created in the graphene devices using the electrical breakdown technique, as described in previous studies[9,28,29]. The graphene gaps were first characterized at room- and low temperature, before deposition of the molecules. Only junctions with resistances higher than 1GΩ and showing no gate dependence were selected for further use. After characterization of the empty gaps, the devices were immersed for 20 hours at 80 degrees in a solution containing dry toluene and the molecules of interest (0.1 mM). The samples were then successively rinsed with dichloromethane, acetone and isopropanol. In the case of the BPC molecule, 46 gaps were formed by electrical breakdown. 29 gaps were characterized at both low and room temperature. After deposition, 23 of these junctions were measured and 9 out of the 23 showed a signal after transfer.

Molecular Dynamic: In order to understand how the 3-carbazolylpropyltrimethoxysilane molecules are interacting with graphene electrodes, molecular dynamic simulation was carried out using ADF[30] reaxFF package. The Velocity Verlet+Berendsen MD method were used with 0.250 fs time step. The atomic positions belong to the SiO_2 substrate and a part of graphene electrodes far from scattering region were constrained. The simulation run for 150000 MD-iterations. The snapshot of atomic coordinates of the junction were taken. These coordinates were used as initial geometries of the device for the density functional theory calculations.

Density functional theory calculation: The optimized geometry and ground state Hamiltonian and overlap matrix elements of each structure studied in this paper were self-consistently obtained using the SIESTA[26] implementation of the density functional theory (DFT). SIESTA employs norm-conserving pseudo-potentials to account for the core electrons and linear combinations

of atomic orbitals (LCAO) to construct the valence states. The generalized gradient approximation (GGA) of the exchange and correlation functional is used with the Perdew-Burke-Ernzerhof (PBE) parameterization and a double-ζ polarized (DZP) basis set. The real-space grid is defined with an equivalent energy cut-off of 250 Ry. The geometry optimization for each structure is performed to the forces smaller than 20 meV/$\mathring{A}$.

Transport: The mean-field Hamiltonian obtained from the converged SIESTA DFT calculation was combined with Gollum[27] implementation of the non-equilibrium Greens function method, to calculate the phase-coherent, elastic scattering properties of the each system consist of left (source) and right (drain) graphene leads connected to the scattering region formed from 3-carbazolylpropyltri-methoxysilane molecules. The transmission coefficient $T(E)$ for electrons of energy E (passing from the source to the drain) is calculated via the relation $T(E) = trace(\Gamma_R(E)G^R(E)\Gamma_L G^{R\dagger}(E))$. In this expression, $\Gamma_{L,R} = i(\Sigma_L, R(E) - \Sigma_L, R^\dagger(E))$ describe the level broadening due to the coupling between left (L) and right (R) electrodes and the central scattering region, are the retarded self-energies associated with this coupling and $G^R = (ES - H - \Sigma_L - \Sigma_R)^{-1}$ is the retarded Greens function, where H is the Hamiltonian and S is the overlap matrix. Using the obtained transmission coefficient, the conductance is calculated by Landauer formula $G = G_0 \int dET(E)(-\partial f(E,\mathrm{T})\partial E)$ where $G_0 = 2e^2/h$ is the conductance quantum, $f(E,\mathrm{T}) = (1 + exp((E - E_F)/k_B\mathrm{T})^{-1}$ is the Fermi-Dirac distribution function, T is the temperature and $k_B = 8.6^{-5}$ eV/K is Boltzmanns constant.

Author contributions

M.E conducted the measurements and performed the data analysis. O.B. and M.E. fabricated the devices. X.L, S-X.L., S.D and S.Y provided the molecules. S.S and H.S provided the theory and performed the DFT calculations. M.E., M.P., H.S., H.S.J.Z., C.L and M.C. designed and supervised the study. M.E., M.P., S.S. and H.S. wrote the paper. M.E., M.P., S.S., H.S., M.C. participated in the discussion of the data. All authors discussed the results and commented the manuscript.

Competing interests The authors declare no competing financial interests.

Materials & **Correspondence** Correspondence and request of materials regarding theoretical

calculations should be addressed to H.S, regarding the synthesis to S-X.L. and those regarding the experiments to M.C.

Data and availability The data that support the plots within this paper and other findings of this study are available from the corresponding authors upon reasonable request. Measurements and analysis were performed in Origin and Matlab. All codes are available from the authors upon reasonable request.

---

* Electronic address: shi-xia.liu@dcb.unibe.ch

† Electronic address: h.sadeghi@lancaster.ac.uk

‡ Electronic address: michel.calame@empa.ch

[1] Visions for a molecular future. *Nature Nanotechnology* **8**, 385–389 (2013). URL http://www.nature.com/doifinder/10.1038/nnano.2013.101.

[2] Aradhya, S. V. & Venkataraman, L. Single-molecule junctions beyond electronic transport. *Nature nanotechnology* **8**, 399–410 (2013).

[3] Sadeghi, H., Sangtarash, S. & Lambert, C. Robust molecular anchoring to graphene electrodes. *Nano Letters* **17**, 4611–4618 (2017).

[4] Tao, N. Electron transport in molecular junctions. *Nature nanotechnology* **1**, 173–181 (2006).

[5] Lau, C. S. *et al.* Redox-dependent franck–condon blockade and avalanche transport in a graphene–fullerene single-molecule transistor. *Nano letters* **16**, 170–176 (2015).

[6] Barreiro, A., van der Zant, H. S. & Vandersypen, L. M. Quantum dots at room temperature carved out from few-layer graphene. *Nano letters* **12**, 6096–6100 (2012).

[7] Sadeghi, H. *et al.* Conductance enlargement in picoscale electroburnt graphene nanojunctions. *Proceedings of the National Academy of Sciences* **112**, 2658–2663 (2015).

[8] Gehring, P. *et al.* Quantum interference in graphene nanoconstrictions. *Nano letters* **16**, 4210–4216 (2016).

[9] Prins, F. *et al.* Room-temperature gating of molecular junctions using few-layer graphene nanogap electrodes. *Nano letters* **11**, 4607–4611 (2011).

[10] Jia, C. *et al.* Covalently bonded single-molecule junctions with stable and reversible photo-

switched conductivity. *Science* **352**, 1443–1445 (2016).

[11] Su, T. A., Neupane, M., Steigerwald, M. L., Venkataraman, L. & Nuckolls, C. Chemical principles of single-molecule electronics. *Nature Reviews Materials* **1**, 16002 (2016).

[12] Li, S. *et al.* The evolving quality of frictional contact with graphene. *Nature* **539**, 541–545 (2016).

[13] Mol, J. A. *et al.* Graphene-porphyrin single-molecule transistors. *Nanoscale* **7**, 13181–13185 (2015).

[14] Xu, Q. *et al.* Single electron transistor with single aromatic ring molecule covalently connected to graphene nanogaps. *Nano letters* **17**, 5335–5341 (2017).

[15] Yao, J., Zhong, L., Natelson, D. & Tour, J. M. Silicon oxide: A non-innocent surface for molecular electronics and nanoelectronics studies. *Journal of the American Chemical Society* **133**, 941–948 (2011).

[16] Pósa, L. *et al.* Multiple physical time scales and dead time rule in few-nanometers sized graphene–sio x-graphene memristors. *Nano letters* **17**, 6783–6789 (2017).

[17] Aswal, D., Lenfant, S., Guerin, D., Yakhmi, J. & Vuillaume, D. Self assembled monolayers on silicon for molecular electronics. *Analytica Chemica Acta* **568**, 84–108 (2006).

[18] DiBenedetto, S. A., Facchetti, A., Ratner, M. A. & Marks, T. J. Molecular self-assembled monolayers and multilayers for organic and unconventional inorganic thin-film transistor applications. *Advanced Materials* **21**, 1407–1433 (2009).

[19] Krasnoslobodtsev, A. V. & Smirnov, S. N. Effect of water on silanization of silica by trimethoxysilanes. *Langmuir* **18**, 3181–3184 (2002).

[20] Hines, T. *et al.* Transition from tunneling to hopping in single molecular junctions by measuring length and temperature dependence. *Journal of the American Chemical Society* **132**, 11658–11664 (2010).

[21] Segal, D., Nitzan, A., Davis, W. B., Wasielewski, M. R. & Ratner, M. A. Electron transfer rates in bridged molecular systems 2. a steady-state analysis of coherent tunneling and thermal transitions. *The Journal of Physical Chemistry B* **104**, 3817–3829 (2000).

[22] Kim, H. & Segal, D. Controlling charge transport mechanisms in molecular junctions: Distilling thermally induced hopping from coherent-resonant conduction. *The Journal of chemical physics* **146**, 164702 (2017).

[23] Hihath, J. Charge transport in the inverted marcus region. *Nature nanotechnology* 1 (2018).

[24] Yuan, L. *et al.* Transition from direct to inverted charge transport marcus regions in molecular junctions via molecular orbital gating. *Nature nanotechnology* 1 (2018).

[25] Selzer, Y., Cabassi, M. A., Mayer, T. S. & Allara, D. L. Thermally activated conduction in molecular junctions. *Journal of the American Chemical Society* **126**, 4052–4053 (2004).

[26] Soler, J. M. *et al.* The siesta method for ab initio order-n materials simulation. *Journal of Physics: Condensed Matter* **14**, 2745 (2002).

[27] Ferrer, J. *et al.* Gollum: a next-generation simulation tool for electron, thermal and spin transport. *New Journal of Physics* **16**, 093029 (2014).

[28] Nef, C. *et al.* High-yield fabrication of nm-size gaps in monolayer cvd graphene. *Nanoscale* **6**, 7249–7254 (2014).

[29] El Abbassi, M. *et al.* From electroburning to sublimation: substrate and environmental effects in the electrical breakdown process of monolayer graphene. *Nanoscale* **9**, 17312–17317 (2017).

[30] K. Chenoweth, A.C.T. van Duin & W.A. Goddard. Reaxff reactive force field for molecular dynamics simulations of hydrocarbon oxidation. *Journal of Physical Chemistry A* **112**, 1040–1053 (2008).

Acknowledgments

We would like to thank Christian Schönenberger for fruitful discussions. This work was partially supported by the EC FP7-ITN MOLESCO grant (N° 606728) and the FET open project QuIET (N° 767187). This work was supported by U.K. EPSRC Grant EP/M014452/1 and EP/N017188/1 and the ERC Advanced grant (Mols@Mols). H.S. acknowledges the UKRI for Future Leaders Fellowship N° MR/S015329/1 and the Leverhulme Trust for Leverhulme Early Career Fellowship N° ECF-2017-186. S.S acknowledges the Leverhulme Trust for Early Career Fellowship N° ECF-2018-375. M.P. acknowledges the funding by the EMPAPOSTDOCS-II programme which has received funding from the European Unions Horizon 2020 research and innovation programme under the Marie Skodowska-Curie Grant Agreement N° 754364. O.B. acknowledges technical support from the Binning and Rohrer Nanotechnology Center (BRNC).